THE ASTROPHYSICAL JOURNAL, 567:391–406, 2002 March 1
© 2002. The American Astronomical Society. All rights reserved. Printed in U.S.A.

OBSERVATIONS OF H_3^+ IN THE DIFFUSE INTERSTELLAR MEDIUM

B. J. MCCALL,[1,2] K. H. HINKLE,[3] T. R. GEBALLE,[4] G. H. MORIARTY-SCHIEVEN,[5] N. J. EVANS II,[6] K. KAWAGUCHI,[7] S. TAKANO,[8] V. V. SMITH,[9] AND T. OKA[1]

Received 2001 June 5; accepted 2001 October 30

ABSTRACT

Surprisingly large column densities of H_3^+ have been detected using infrared absorption spectroscopy in seven diffuse cloud sight lines (Cygnus OB2 12, Cygnus OB2 5, HD 183143, HD 20041, WR 104, WR 118, and WR 121), demonstrating that H_3^+ is ubiquitous in the diffuse interstellar medium. Using the standard model of diffuse cloud chemistry, our H_3^+ column densities imply unreasonably long path lengths ($\sim$1 kpc) and low densities ($\sim$3 cm^{-3}). Complimentary millimeter-wave, infrared, and visible observations of related species suggest that the chemical model is incorrect and that the number density of H_3^+ must be increased by 1–2 orders of magnitude. Possible solutions include a reduced electron fraction, an enhanced rate of H_2 ionization, and/or a smaller value of the H_3^+ dissociative recombination rate constant than implied by laboratory experiments.

Subject headings: cosmic rays — infrared: ISM: lines and bands — ISM: clouds — ISM: molecules — molecular processes

1. INTRODUCTION

The H_3^+ molecular ion has long been considered to play an important role in the chemistry of dense molecular clouds, since it initiates the network of ion-neutral reactions (Herbst & Klemperer 1973; Watson 1973) that is responsible for the wealth of molecules observed by radio and infrared astronomers. However, H_3^+ has not been considered to be an important species in diffuse clouds, because it is thought to be destroyed rapidly by dissociative recombination with electrons, which are abundant in diffuse clouds. For the purposes of the present study, we do not make a distinction between diffuse and translucent clouds but simply use "diffuse" to indicate sight lines where CO is not the dominant reservoir of carbon (in contrast to dense clouds).

The detection of H_3^+ in the diffuse interstellar medium toward the Galactic center (Geballe et al. 1999) and toward the visible star Cygnus OB2 12 (McCall et al. 1998a) with column densities similar to those of dense clouds (McCall et al. 1999) was therefore quite surprising. These observational results imply either a very long path length (hundreds of parsecs) of absorbing material or a serious problem with the standard model of diffuse cloud chemistry. Various attempts have been made to explain the abundance of H_3^+ toward Cygnus OB2 12 while preserving the standard model of the chemistry, either by adjusting all parameters to optimize H_3^+ (Cecchi-Pestellini & Dalgarno 2000) or by postulating an additional ionization source for H_2 molecules peculiar to the neighborhood of the Cygnus OB2 association (Black 2000).

We have conducted a small survey of twelve diffuse cloud sources with the aim of determining whether the sight line toward Cygnus OB2 12 is unique, or whether high column densities of H_3^+ are common in diffuse clouds. As a result of this survey, we have detected H_3^+ in seven diffuse cloud sources (Cygnus OB2 12, Cygnus OB2 5, HD 183143, HD 20041, WR 104, WR 118, and WR 121) and obtained upper limits toward five other sources (HD 194279, HD 168607, P Cygni, χ^2 Ori, and ζ Oph). For Cygnus OB2 12 and 5 and HD 181343, we have also obtained infrared and radio spectra of CO, as well as high-resolution visible spectra of relevant atoms and molecules. We have also obtained infrared CO spectra toward WR 104 and WR 108.

These results demonstrate the ubiquity of H_3^+ in diffuse clouds and suggest that there is a "global" problem with the current models. In this respect, H_3^+ represents a major problem in diffuse cloud chemistry, reminiscent of the diffuse interstellar bands and CH^+.

2. OBSERVATIONS AND DATA REDUCTION

The stellar parameters of our targets are listed in Table 1, and a summary of the observations is provided in Table 2. The $R(1, 1)^l$ line of H_3^+ at 3.715 μm was observed using the Phoenix spectrometer on the Mayall 4 m telescope at Kitt Peak National Observatory (KPNO). The H_3^+ observations were performed in three runs (1998 July, 2000 June, and 2001 March). The CGS4 facility spectrometer on the United Kingdom Infrared Telescope (UKIRT) was used in 2000 July and 2001 May to study the $R(1, 0)$–$R(1, 1)^u$ doublet of H_3^+ near 3.668 μm. The three observed H_3^+ rotation-vibration transitions belong to the fundamental band of the ν_2 degenerate bending mode and arise from the lowest allowed rotational states $(J, K) = (1, 1)$ and $(1, 0)$. The old notation [e.g., $R(1, 1)^+$] has been superseded by a more flexible notation [e.g., $R(1, 1)^u$] that uses u and l in place of + and − (for a complete description of the new standard notation for H_3^+, see McCall 2000 or McCall & Oka 2000).

[1] Department of Chemistry, Department of Astronomy and Astrophysics, and the Enrico Fermi Institute, University of Chicago, Chicago, IL 60637.

[2] Present address: Department of Astronomy, University of California at Berkeley, 601 Campbell Hall, Berkeley, CA 94720; bjmccall@astro.berkeley.edu.

[3] National Optical Astronomy Observatory, 950 North Cherry Avenue, Tucson, AZ 85726.

[4] Gemini Observatory, 670 North A'ohoku Place, Hilo, HI 96720.

[5] Joint Astronomy Centre, 660 North A'ohoku Place, Hilo, HI 96720.

[6] Department of Astronomy, University of Texas at Austin, Austin, TX 78712-1083.

[7] Faculty of Science, Okayama University, 3-1-1, Tsushima-naka, Okayama 700-8530, Japan.

[8] Nobeyama Radio Observatory, Minamimaki, Minamisaku, Nagano 384-1305, Japan.

[9] Department of Physics, University of Texas at El Paso, El Paso, TX 79968; and McDonald Observatory, University of Texas at Austin, Austin, TX 78712.

TABLE 1

STELLAR PARAMETERS

Name	V	$E(B-V)$	Spectral Type	Distance (pc)
WR 118	22.0	4.13[a]	WC9	6300[b]
Cyg OB2 12.....	11.4	3.35[c]	B5 Iab	1700[d]
WR 104	13.5	2.10[a]	WC9	1300[b]
Cyg OB2 5	9.2	1.99[c]	O7e	1700[d]
WR 121	11.9	1.68[a]	WC9	1690[b]
HD 168607.....	8.25	1.61[e]	B9 Ia	1100[f]
HD 183143.....	6.9	1.28[e]	B7 Ia	1000[f]
HD 194279.....	7.1	1.22[e]	B1.5 Ia	1100[f]
HD 20041	5.8	0.70[g]	A0 Ia	1400[f]
P Cygni	4.8	0.63[h]	B2pe	1800[h]
χ^2 Ori.....	4.6	0.44[i]	B2 Iae	1000[f]
ζ Oph	2.6	0.32[e]	O9 V	140[j]

[a] From Pendleton et al. 1994, assuming $R_V = A_V/E(B-V) = 3.1$.
[b] Smith et al. 1990.
[c] From Schulte 1958.
[d] Torres-Dodgen, Carroll, & Tapia 1991.
[e] From Snow, York, & Welty 1977.
[f] Our estimate (spectroscopic parallax).
[g] Racine 1968.
[h] From Lamers, de Groot, & Cassatella 1983.
[i] From the intrinsic color of Wegner 1994.
[j] From *Hipparcos* catalog (Perryman et al. 1997).

Infrared spectra of portions of the fundamental ($v = 1$–0) and overtone ($v = 2$–0) infrared bands of CO were also obtained. The fundamental band was studied toward Cygnus OB2 12 and Cygnus OB2 5 with Phoenix in 1999 July and 2000 June and toward HD 183143, WR 104, and WR 118 with CGS4 in 2001 May. The overtone band of CO was searched for with Phoenix toward HD 183143 in 1997 June and toward Cygnus OB2 12 in 1999 July.

All the infrared data were reduced using the procedure outlined in McCall et al. (1999), which is described in more detail in McCall (2001).[10] Object spectra were ratioed by (scaled) standard spectra in order to remove the many strong atmospheric absorption lines in these regions. The wavelength calibration was achieved using telluric absorption lines and is estimated to be accurate to roughly 2 km s^{-1}. The resolving power of the Phoenix spectrometer was roughly 40,000 until 1998 and approximately 60,000 during 1999–2001. The CGS4 spectrometer was used with the long camera, yielding a resolving power of 40,000.

High-resolution visible spectra of atoms and molecules of interest were obtained using the coudé spectrometer on the Smith 2.7 m telescope at McDonald Observatory. A total of three echelle settings were used. The first covered the K I line at 7699 Å and the CN A-X $v = 2$–0 $R_2(0)$ line at 7875 Å. The second covered the C_2 A-X $v = 2$–0 band near 8760 Å. These two echelle settings were used with the F1E2 configuration and the 0.″2 slit, which yielded a resolving power of about 200,000. The third echelle setting covered Ca I at 4227 Å, Ca II at 3934 Å, CH at 4300 Å, CH^+ at 4232 Å, and CN B-X $v = 0$–0 near 3874 Å. This setting was used with the F1E1 configuration and the 0.″6 slit, to yield a resolving power of approximately 120,000. The McDonald data were reduced using standard IRAF routines (CCDPROC and DOECSLIT). It was not generally necessary to ratio the visible spectra by standard stars, because of the weakness and paucity of atmospheric absorption lines in the regions of interest. Wavelength calibration was achieved using comparison spectra of a Th-Ar lamp and is estimated to be good to about 0.01 Å in all cases.

Rotational spectra of CO in the Cygnus OB2 association were obtained at the Nobeyama Radio Observatory (NRO) for $J = 1$–0 and the Caltech Submillimeter Observatory (CSO) for $J = 2$–1 and 3–2. The CSO spectra were obtained using position switching with an "off" position of 30′ south. This position has significant ^{12}CO emission but no detectable ^{13}CO emission compared with a more distant off position, which is important since the ^{13}CO data is used in the interpretation of the infrared CO lines. The NRO spectra were obtained using position switching with an off position of ($l = 81$, $b = 3$), which was found to be more free of CO emission. CO spectra toward HD 183143 were also obtained at the James Clerk Maxwell Telescope (JCMT) for $J = 2$–1 and at NRO for $J = 1$–0, using frequency switching. In all cases, data were reduced using the standard procedures.

3. RESULTS

3.1. H_3^+ *Spectra*

In our 1998 observing run at Kitt Peak, we detected H_3^+ for the first time toward Cygnus OB2 5, which lies approximately 6′ (3 pc at 1.7 kpc) away from Cygnus OB2 12. Although the H_3^+ $R(1, 1)^l$ line was unfortunately Doppler shifted under the telluric CH_4 feature near 37152 Å, we are confident that the detection is secure, because the other telluric CH_4 line (near 37158 Å) is removed very effectively by ratioing with a standard star and because we observed a similar H_3^+ feature in Cygnus OB2 12 at the same velocity with an equivalent width consistent with our earlier observations (McCall et al. 1998a). Our Kitt Peak H_3^+ observations are summarized in Figure 1.

Our 1998 run also yielded detections of H_3^+ toward the Wolf-Rayet stars WR 121, WR 104, and WR 118. The source WR 118 is interesting in that it shows two H_3^+ components, which have similar (though not the same) spacing as the two telluric CH_4 lines. Consequently, the scaling and ratioing by the standard star was performed by choosing parameters that minimized the residuals of CH_4 lines elsewhere in the spectrum (not shown in the figure). It is worth noting that the inferred velocities of the peaks ($\sim +5$ and $+48$ km s^{-1}) would occur at heliocentric distances of ~ 0.5 and 3 kpc, respectively, assuming a flat Galactic rotation curve with $v_c = 220$ km s^{-1}, $R_0 = 8$ kpc, and $l = 21.^\circ 80$. These distances do not exceed the estimated distance to the source ($m - M = 14$, or $d \sim 6.3$ kpc) obtained from the observed V magnitude of 22, the visual extinction $A_V = 12.8$ from van der Hucht et al. (1996), and the absolute magnitude $M_V = -4.8$ for WC9 stars (Smith, Shara, & Moffat 1990).

Finally, our 1998 Kitt Peak run yielded a nondetection toward HD 194279, toward which CH is observed with a heliocentric velocity of -11.8 km s^{-1} (G. Galazutdinov 2001, private communication). This source, along with the Wolf-Rayet stars, was chosen for study because the 3.4 μm aliphatic carbon feature (a signature of diffuse clouds) had been detected by Pendleton et al. (1994).

Our 2000 June run at Kitt Peak yielded the first detection of H_3^+ toward a more traditional diffuse cloud source, HD 183143. Two components of H_3^+ were seen, in agreement

[10] Available on-line at http://h3plus.uchicago.edu.

TABLE 2

LOG OF OBSERVATIONS

Date (UT)	Observatory	Species	Transition	Object	Standard	Time (minutes)
1997 Jun 25	KPNO	CO	$v = 2$–0	HD 183143	α Lyr	60
1998 Jul 3	KPNO	H_3^+	$R(1, 1)^l$	Cyg OB2 12	α Cyg	30
1998 Jul 3	KPNO	H_3^+	$R(1, 1)^l$	Cyg OB2 5	α Cyg	164
1998 Jul 4	KPNO	H_3^+	$R(1, 1)^l$	WR 104	α Lyr	35
1998 Jul 4	KPNO	H_3^+	$R(1, 1)^l$	WR 121	α Lyr	112
1998 Jul 4	KPNO	H_3^+	$R(1, 1)^l$	WR 118	α Cyg	46
1998 Jul 4	KPNO	H_3^+	$R(1, 1)^l$	HD 194279	α Cyg	92
1999 Jul 4	KPNO	CO	$v = 2$–0	Cyg OB2 12	α Cyg	4
1999 Jul 5	KPNO	CO	$v = 1$–0	Cyg OB2 12	α Lyr	4
1999 Jul 5	KPNO	CO	$v = 1$–0	Cyg OB2 5	α Lyr	8
2000 Jun 25	KPNO	H_3^+	$R(1, 1)^l$	Cyg OB2 12	α Cyg	60
2000 Jun 25	KPNO	H_3^+	$R(1, 1)^l$	HD 183143	α Lyr	84
2000 Jun 25	KPNO	H_3^+	$R(1, 1)^l$	P Cygni	α Lyr	78
2000 Jun 26	KPNO	H_3^+	$R(1, 1)^l$	ζ Oph	α Lyr	48
2000 Jun 26	KPNO	CO	$v = 1$–0	Cyg OB2 12	α Lyr	36
2000 Jun 26	KPNO	CO	$v = 1$–0	Cyg OB2 5	α Lyr	90
2001 Mar 13	KPNO	H_3^+	$R(1, 1)^l$	HD 20041	α CMa	100
2001 Mar 13	KPNO	H_3^+	$R(1, 1)^l$	χ^2 Ori	α CMa	60
2000 Jul 6	UKIRT	H_3^+	$R(1, 0)$, $R(1, 1)^u$	HD 183143	α Lyr	29
2000 Jul 6	UKIRT	H_3^+	$R(1, 0)$, $R(1, 1)^u$	Cyg OB2 5	α Cyg	43
2000 Jul 7	UKIRT	H_3^+	$R(1, 0)$, $R(1, 1)^u$	HD 168607	π Sgr	25
2001 May 24.....	UKIRT	H_3^+	$R(1, 0)$, $R(1, 1)^u$	WR 104	η Oph	8
2001 May 24.....	UKIRT	H_3^+	$R(1, 0)$, $R(1, 1)^u$	WR 118	α Cyg	6
2001 May 28.....	UKIRT	CO	$v = 1$–0	HD 183143	α Aql	24
2001 May 28.....	UKIRT	CO	$v = 1$–0	WR 104	β^1 Sco	3
2001 May 28.....	UKIRT	CO	$v = 1$–0	WR 118	η Oph	5
2000 Sep 12	McDonald	K I	^2P–^2S	Cyg OB2 12	α Cyg	60
		CN	A-X $v = 2$–0			
2000 Sep 12	McDonald	K I	^2P–^2S	Cyg OB2 5	α Cyg	60
		CN	A-X $v = 2$–0			
2000 Sep 12	McDonald	K I	^2P–^2S	HD 183143	α Cyg	60
		CN	A-X $v = 2$–0			
2000 Sep 12	McDonald	C_2	A-X $v = 2$–0	Cyg OB2 12	α Cep	60
2000 Sep 12	McDonald	C_2	A-X $v = 2$–0	Cyg OB2 5	α Cep	60
2000 Sep 12	McDonald	C_2	A-X $v = 2$–0	HD 183143	α Cep	60
2000 Sep 14	McDonald	Ca I	^1P–^1S	Cyg OB2 5	α Cyg	200
		Ca II	^2P–^2S			
		CH	A-X $v = 0$–0			
		CH^+	A-X $v = 0$–0			
		CN	B-X $v = 0$–0			
2000 Sep 14	McDonald	Ca I	^1P–^1S	HD 183143	α Cyg	100
		Ca II	^2P–^2S			
		CH	A-X $v = 0$–0			
		CH^+	A-X $v = 0$–0			
		CN	B-X $v = 0$–0			
1999 Jul 28.....	CSO	^{12}CO	$J = 2$–1	Cyg OB2 12	30′ S	14
1999 Jul 28.....	CSO	^{12}CO	$J = 2$–1	Cyg OB2 5	30′ S	14
1999 Jul 28–29.....	CSO	^{13}CO	$J = 2$–1	Cyg OB2 12	30′ S	32
1999 Jul 28–29.....	CSO	^{13}CO	$J = 2$–1	Cyg OB2 5	30′ S	32
1999 Jul 28.....	CSO	^{13}CO	$J = 3$–2	Cyg OB2 12	30′ S	20
1999 Jul 28.....	CSO	^{13}CO	$J = 3$–2	Cyg OB2 5	30′ S	20
2000 Apr 9	NRO	^{12}CO	$J = 1$–0	Cyg OB2 12	($l = 81$, $b = 3$)	18
2000 Apr 9	NRO	^{13}CO	$J = 1$–0	Cyg OB2 12	($l = 81$, $b = 3$)	37
2000 Apr 11.....	NRO	^{12}CO	$J = 1$–0	Cyg OB2 "A"	($l = 81$, $b = 3$)	10
2000 Apr 11.....	NRO	^{12}CO	$J = 1$–0	Cyg OB2 "B"	($l = 81$, $b = 3$)	10
2000 Apr 11.....	NRO	^{12}CO	$J = 1$–0	Cyg OB2 "C"	($l = 81$, $b = 3$)	15
2000 Apr 11.....	NRO	^{12}CO	$J = 1$–0	Cyg OB2 "D"	($l = 81$, $b = 3$)	10
2000 Apr 14.....	NRO	^{12}CO	$J = 1$–0	Cyg OB2 5	($l = 81$, $b = 3$)	13
2000 Oct 13.....	JCMT	^{12}CO	$J = 2$–1	HD 183143	(8 MHz)	60
2000 Oct 13.....	JCMT	^{12}CO	$J = 2$–1	HD 183143	(16 MHz)	60
2000 Dec 14	NRO	^{12}CO	$J = 1$–0	HD 183143	(3 MHz)	12
2000 Dec 14	NRO	^{12}CO	$J = 1$–0	HD 183143	(6 MHz)	13
2000 Dec 15	NRO	^{12}CO	$J = 1$–0	HD 183143	(4 MHz)	31
2000 Dec 15	NRO	^{12}CO	$J = 1$–0	HD 183143	(9 MHz)	45

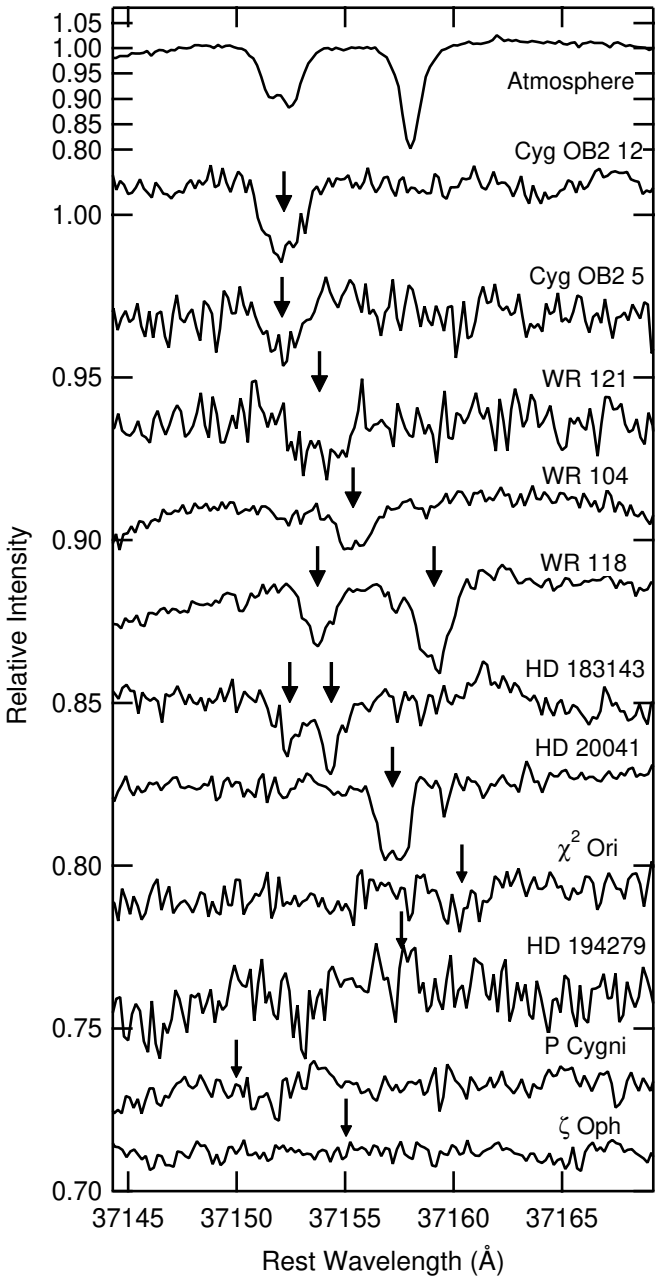

FIG. 1.—Spectra of the H_3^+ $R(1, 1)^l$ line observed with Phoenix at Kitt Peak. Each object spectrum has been ratioed by that of a standard star to remove atmospheric absorption lines. The vertical arrows denote the observed (*thick arrows*) or expected (*thin arrows*) positions of H_3^+ depending on each source's Doppler shift at the time of observation.

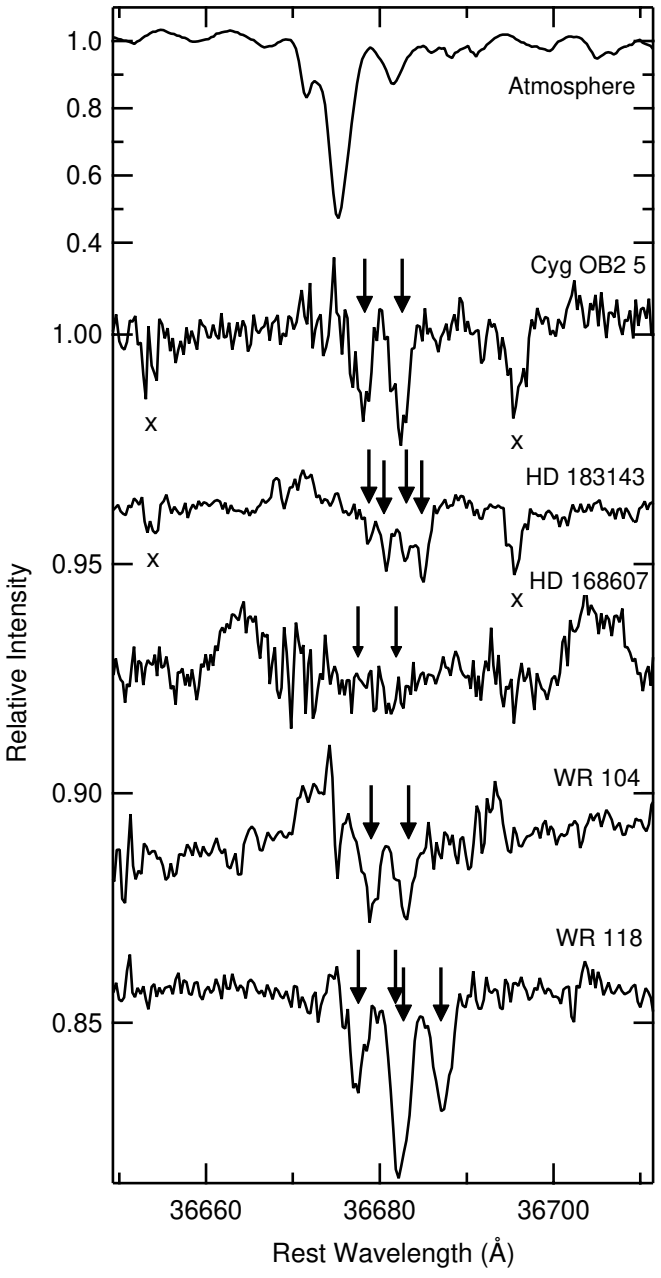

FIG. 2.—Spectra of the H_3^+ $R(1, 0)$–$R(1, 1)^u$ doublet of H_3^+ observed with CGS4 at UKIRT. Each object spectrum has been ratioed by that of a standard star to remove atmospheric absorption lines. The vertical arrows denote the observed or expected (for HD 168607) position of the H_3^+ doublet. The crosses label instrumental artifacts.

with the visible spectra of other molecules (see below), although the blue component was somewhat affected by the telluric CH_4 line. During this run, we also obtained nondetections toward P Cygni (which has an LSR velocity of CH^+ of -9 km s^{-1}; Hobbs 1973) and toward ζ Oph (which has an LSR velocity of CO of -0.79 km s^{-1}; Lambert, Sheffer, & Crane 1990). Our 2001 March run at Kitt Peak yielded a detection of H_3^+ toward the least reddened star to date, HD 20041. We also obtained an upper limit of H_3^+ absorption toward χ^2 Ori.

Our run at UKIRT in 2000 July (see Fig. 2) confirmed the detections of H_3^+ toward Cygnus OB2 5 and HD 183143. In the case of HD 183143, the two-component velocity structure is very clear. For both the Cygnus OB2 5 and HD 183143 observations, instrumental artifacts were present in the "negative" spectrum—these features changed in intensity (and sometimes disappeared) depending on exactly which rows of the array were extracted, while the H_3^+ features were consistently present. We also obtained a nondetection toward HD 168607 (which has a heliocentric CH velocity of 22 km s^{-1}; Gredel 1999).

In 2001 May at UKIRT, we confirmed the detections of H_3^+ toward the Wolf-Rayet stars WR 104 and WR 108 by using the $R(1, 1)^u$–$R(1, 0)$ doublet. The separation of the two velocity components toward WR 118 is comparable to the spacing between the two H_3^+ transitions, so that the $R(1, 0)$

of the blue component and the $R(1, 1)^u$ of the red component are overlapped.

A table of the observed H_3^+ line parameters is given in Table 3. The observed equivalent widths have been converted to column densities under the assumption that the lines are optically thin, using the transition dipole moments calculated by J. K. G. Watson, as listed in McCall et al. (1998a).

3.2. CO *toward the Cygnus OB2 Association*

A brief look at the high-resolution infrared spectrum of CO toward Cygnus OB2 12 and Cygnus OB2 5 was obtained during test and engineering time with Phoenix at Kitt Peak in 1999 July. Follow-up observations with longer integration time in 2000 June yielded higher signal-to-noise ratio spectra, displayed in Figure 3. The observations of Cygnus OB2 12 clearly show the two closely spaced (~ 5 km s^{-1}) velocity components observed in the millimeter-wave spectrum from JCMT (Geballe et al. 1999). The infrared lines suggest a CO excitation temperature of ~ 10 K toward Cygnus OB2 12, but this should not be taken as an indication of the kinetic temperature of the gas because of the effect of spontaneous emission (Geballe et al. 1999). The infrared CO line parameters are listed in Table 4. We have adopted the transition dipole moments of Huré & Roueff (1996).

The signal-to-noise ratio of the Cygnus OB2 12 spectrum is clearly not high enough to rely on the measured equivalent widths of the individual components, particularly because of the contamination of the telluric lines. However, we can estimate the column density of CO by assuming that the true equivalent widths of the two components have the same ratio as the integrated areas of the components in the ^{13}CO emission spectrum and by adopting the b-values of the ^{13}CO in estimating the saturation corrections. This analysis was performed with the high-quality ^{13}CO spectrum obtained at CSO (shown in Fig. 4; the millimeter-wave line parameters are listed in Table 5). We assume that the 7 km s^{-1} peak carries 0.39 of the equivalent width (and has $b = 0.75$ km s^{-1}) and that the 12 km s^{-1} peak carries 0.61 of the equivalent width (and has $b = 0.88$ km s^{-1}). With these assumptions we estimate a total CO column density of $\sim 1.4 \times 10^{17}$ cm^{-2} in front of Cygnus OB2 12. This estimate is considerably higher than the estimate of 3×10^{16} cm^{-2} given in Geballe et al. (1999) but still much lower than the total column density of carbon ($\sim 2.5 \times 10^{18}$ cm^{-2}) inferred from the color excess.

We have also obtained an upper limit on the CO column density toward Cygnus OB2 12, based on our failure to detect the $v = 2$–0 overtone with Phoenix. The upper limit on the $v = 2$–0 features yields an upper limit (3 σ) of $N(\mathrm{CO}) \lesssim 3 \times 10^{17}$ cm^{-2}. This suggests that at most about

TABLE 3

H_3^+ LINE PARAMETERS

Object	Line	v_{LSR} (km s^{-1})	FWHM (km s^{-1})	W_λ (Å)	$\sigma(W_\lambda)$[a] (Å)	$N(H_3^+)$ (10^{14} cm^{-2})	$\sigma(N)$[a] (10^{14} cm^{-2})
Cyg OB2 12.....	$R(1, 1)^l$	7.0	14.6	0.044	0.002	2.02	0.09
Cyg OB2 5.....	$R(1, 1)^l$	7.3	11.5	0.022	0.003	0.99	0.15
	$R(1, 1)^u$	5.6	15.2	0.035	0.004	1.43	0.16
	$R(1, 0)$	5.8	15.4	0.048	0.004	1.21	0.10
WR 121	$R(1, 1)^l$	9.7	17.8	0.024	0.004	1.12	0.20
WR 104	$R(1, 1)^l$	10.9	15.1	0.028	0.002	1.27	0.07
	$R(1, 1)^u$	11.2	14.6	0.030	0.005	1.23	0.21
	$R(1, 0)$	7.9	18.5	0.041	0.006	1.05	0.14
WR 118	$R(1, 1)^l$	4.8	9.5	0.019	0.001	0.89	0.06
		47.6	12.3	0.041	0.002	1.88	0.07
	$R(1, 1)^u$	3.7	17.1	0.045	0.003	1.86	0.11
		44.3[b]	15.4	0.026	0.002	1.06	0.10
	$R(1, 0)$	8.5[b]	21.7	0.077	0.003	1.95	0.07
		48.1	19.6	0.065	0.003	1.64	0.07
HD 183143.....	$R(1, 1)^l$	8.3[c]	10.5	0.020	0.002	0.94	0.08
		23.6	8.4	0.024	0.002	1.10	0.07
	$R(1, 1)^u$	7.1	12.2	0.012	0.001	0.50	0.05
		23.4	9.9	0.017	0.001	0.70	0.05
	$R(1, 0)$	5.6	14.0	0.022	0.001	0.54	0.03
		22.1	11.0	0.023	0.001	0.59	0.03
HD 20041	$R(1, 1)^l$	−0.5	11.5	0.038	0.002	1.74	0.09
HD 194279.....	$R(1, 1)^l$	...	10[d]	...	0.005	...	0.21[e]
P Cygni	$R(1, 1)^l$	...	10[d]	...	0.002	...	0.10[e]
ζ Oph.....	$R(1, 1)^l$	...	10[d]	...	0.001	...	0.06[e]
HD 168607.....	$R(1, 1)^u$	...	10[d]	...	0.003	...	0.13[e]
	$R(1, 0)$	...	10[d]	...	0.003	...	0.07[e]
χ^2 Ori.....	$R(1, 1)^l$	...	10[d]	...	0.003	...	0.12[e]

[a] Statistical uncertainties (1 σ) are listed. Systematic errors (for instance, due to ratioing of telluric lines) are difficult to estimate and are likely larger.

[b] These two features are overlapped, so the fit results are highly uncertain.

[c] Affected by telluric line.

[d] Adopted FWHM for purposes of computing upper limits.

[e] The firm upper limit for $N(H_3^+)$ should be considered to be 3 σ.

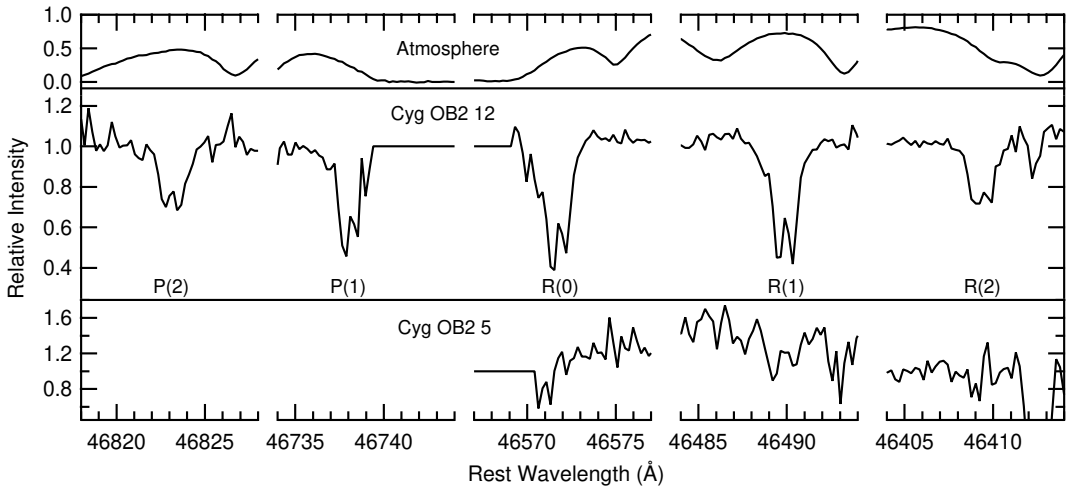

FIG. 3.—Infrared $v = 1$–0 CO spectra obtained with Phoenix at Kitt Peak. Object spectra have been ratioed by standard star spectra to remove the atmospheric CO lines. The horizontal segments of the spectra indicate regions where the strong telluric absorptions could not be ratioed out.

TABLE 4

INFRARED ^{12}CO $v = 1$–0 LINE PARAMETERS

Object	Line	v_{LSR} (km s^{-1})	FWHM (km s^{-1})	W_λ (Å)	$\sigma(W_\lambda)$[a] (Å)	N(thin)[b] (10^{15} cm^{-2})	$\sigma(N)$[a] (10^{15} cm^{-2})
Cyg OB2 12.....	*P*2	5.9	4.3	0.199	0.021	2.28	0.24
		11.8	6.1	0.300	0.025	3.42	0.29
	*P*1	6.0	4.1	0.344	0.024	4.71	0.32
		10.3[c]	1.8	0.127	0.015	1.74	0.21
	*R*0	7.5	6.0	0.598	0.029	2.75	0.13
		13.1	3.8	0.285	0.023	1.31	0.11
	*R*1	6.6	4.6	0.437	0.021	3.01	0.15
		12.0	3.9	0.355	0.019	2.45	0.13
	*R*2	7.6	5.1	0.248	0.010	1.91	0.08
		13.1	4.9	0.185	0.010	1.42	0.08
Cyg OB2 5	*R*1[d]	4.9	4.8	0.303	0.041	2.09	0.29
		12.2	4.5	0.204	0.041	1.40	0.28
HD 183143.....	*R*0	25.6	13.0	0.138	0.013	0.64	0.06
	*R*1[d]	24.4	16.1	0.133	0.010	0.91	0.07
WR 104	*R*0	21.4	12.9	0.520	0.024	2.39	0.11
	*R*1	21.2	12.4	0.588	0.019	4.05	0.13
	*R*2	21.5	7.2	0.247	0.014	1.89	0.11
	*R*3	20.6	5.1	0.143	0.011	1.16	0.09
WR 118	*R*0	10.5	18.2	1.289	0.020	5.93	0.09
		45.0[e]	18.0	1.147	0.020	5.28	0.09
		59.4[e]	15.6	0.198	0.018	0.91	0.08
		85.0	14.0	0.107	0.017	0.49	0.08
	*R*1	9.2	16.6	0.962	0.015	6.63	0.10
		41.6[e]	15.1	1.078	0.014	7.43	0.10
		56.9[e]	10.5	0.204	0.012	1.41	0.08
		81.6	15.1	0.211	0.015	1.45	0.10
	*R*2	9.1	12.8	0.248	0.013	1.90	0.10
		41.7[e]	10.6	0.539	0.012	4.13	0.09
		53.6[e]	13.2	0.111	0.013	0.85	0.10
		82.9	11.1	0.144	0.012	1.10	0.09
	*R*3	36.4	19.1	0.219	0.010	1.77	0.08
		82.3	12.5	0.097	0.008	0.78	0.06

[a] Statistical uncertainties (1 σ) are listed. Systematic errors (for instance, due to ratioing of telluric lines) are difficult to estimate and may be larger.

[b] Listed column densities are for the lower state of each absorption line in the given velocity component. These are direct calculations from the corresponding value of W_λ, in the optically thin limit. For a more detailed analysis of the CO column density toward Cygnus OB2 12, see § 3.2.

[c] Bad fit due to interference of telluric line.

[d] Other lines too marginal to fit.

[e] Blend of two components; individual fit parameters uncertain.

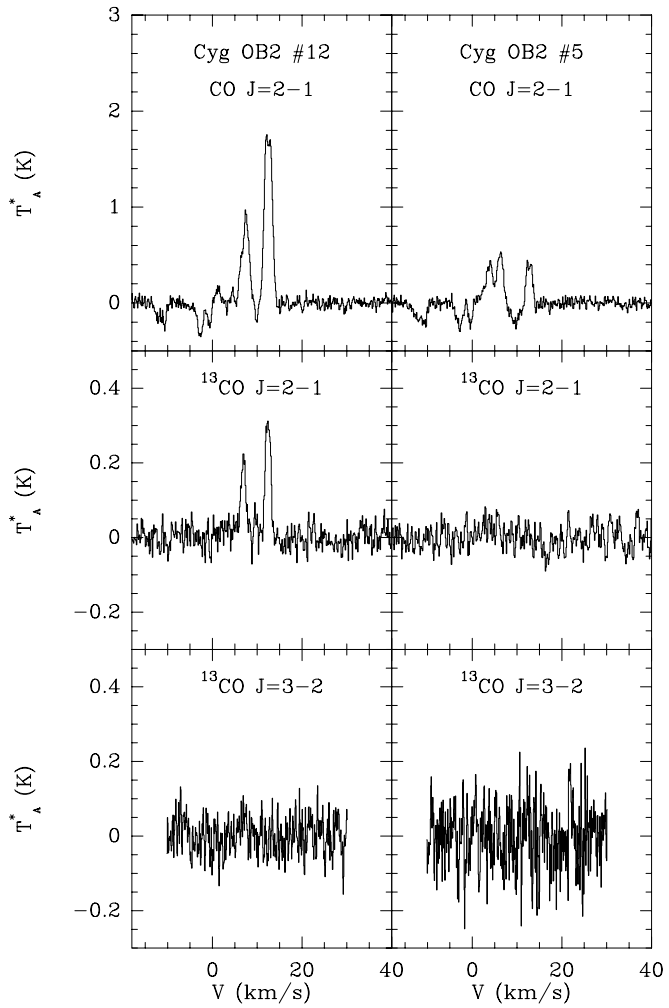

FIG. 4.—CO spectra obtained at CSO

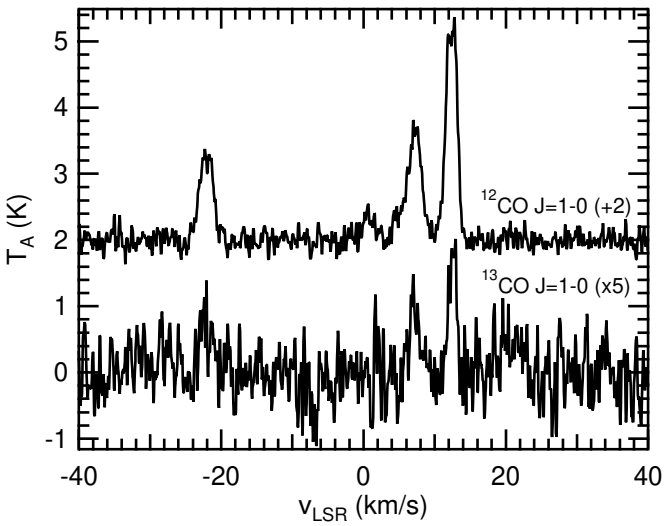

FIG. 5.—CO $J = 1$–0 spectra of Cygnus OB2 12 obtained at NRO

10% of the carbon along the line of sight to Cygnus OB2 12 can be in the form of CO and that this sight line does not consist of dense clouds.

Using the ^{13}CO data from CSO for $J = 2$–1 and from NRO for $J = 1$–0 (see Fig. 5), we performed an analysis using an LVG code to calculate the statistical equilibrium, assuming a temperature of about 30 K (consistent with the C_2 analysis of § 3.5 and the H_3^+ analysis of § 4.2). If the density ($n = 200$ cm^{-3}) derived from the analysis of C_2 toward Cygnus OB2 12 is assumed, the ^{13}CO column density, $N(13)$, is determined uniquely by matching the observed line emission. The results are $N(13) = 1.8 \times 10^{15}$ cm^{-2} for the 7 km s^{-1} component and $N(13) = 2.7 \times 10^{15}$ cm^{-2} for the 12 km s^{-1} component. The sum of these, $N(13) = 4.5 \times 10^{15}$ cm^{-2}, would imply a total column density of CO of (2.3–4.5) $\times 10^{17}$ cm^{-2} for isotope ratios of 50–100; this column density is about twice that inferred from the infrared CO absorption lines. If, on the other hand, we enforce agreement with the column density from the infrared absorption and assume an isotope ratio of 100, the ^{13}CO data indicate somewhat higher densities: $n = 500$ cm^{-3} for the 7 km s^{-1} component and $n = 900$ cm^{-3} for the 12 km s^{-1} component.

While these densities are somewhat higher than inferred from C_2, it would not be surprising to have density variations, with the ^{13}CO data probing the denser gas and the C_2 probing somewhat less dense gas.

The line of sight toward Cygnus OB2 5 appears to have considerably less CO than that toward Cygnus OB2 12, based both on the marginal detections in the infrared spectrum (Fig. 3) as well as the CSO ^{13}CO spectra (Fig. 4). Therefore, we expect that this sight line is also dominated by diffuse cloud material, although because of the low signal-to-noise ratio of the infrared spectrum it is difficult to estimate the CO column density.

In order to probe the spatial extent of the CO gas in the Cygnus OB2 association, we have obtained (position switched) ^{12}CO $J = 1$–0 spectra at four other locations in the association, labeled A through D in Table 2 and Figure 6, which also shows the spectra toward Cygnus OB2 12 and 5.

TABLE 5

MILLIMETER-WAVE CO TOWARD CYGNUS OB2 12

Species	Line	v_{LSR} (km s^{-1})	HWHM (km s^{-1})	T_A^* (peak) (K)	Area (K km s^{-1})
^{13}CO	$J = 1$–0	6.93	1.30	0.29	0.52
		12.58	1.32	0.41	0.58
	$J = 2$–1	6.9	1.39	0.21	0.31
		12.4	1.35	0.33	0.47
^{12}CO	$J = 1$–0	7.31	2.52	1.49	3.34
		12.72	1.81	3.08	5.98
	$J = 2$–1	7.48	1.92	0.92	1.72
		12.48	2.04	1.74	3.66

3.3. CO *toward HD 183143*

To check for the presence of CO in this sight line, we obtained rotational spectra of the $J = 2$–1 line (at JCMT) and the $J = 1$–0 line (at NRO). The JCMT results (frequency switched at 8 and 16 MHz) are shown in Figure 7. While the $J = 2$–1 spectrum of Cygnus OB2 12 showed nearly 2 K of emission at the H_3^+ velocity, the spectrum of HD 183143 shows no emission at the correct velocities in excess of $\sim$0.1 K. The NRO results are shown in Figure 8

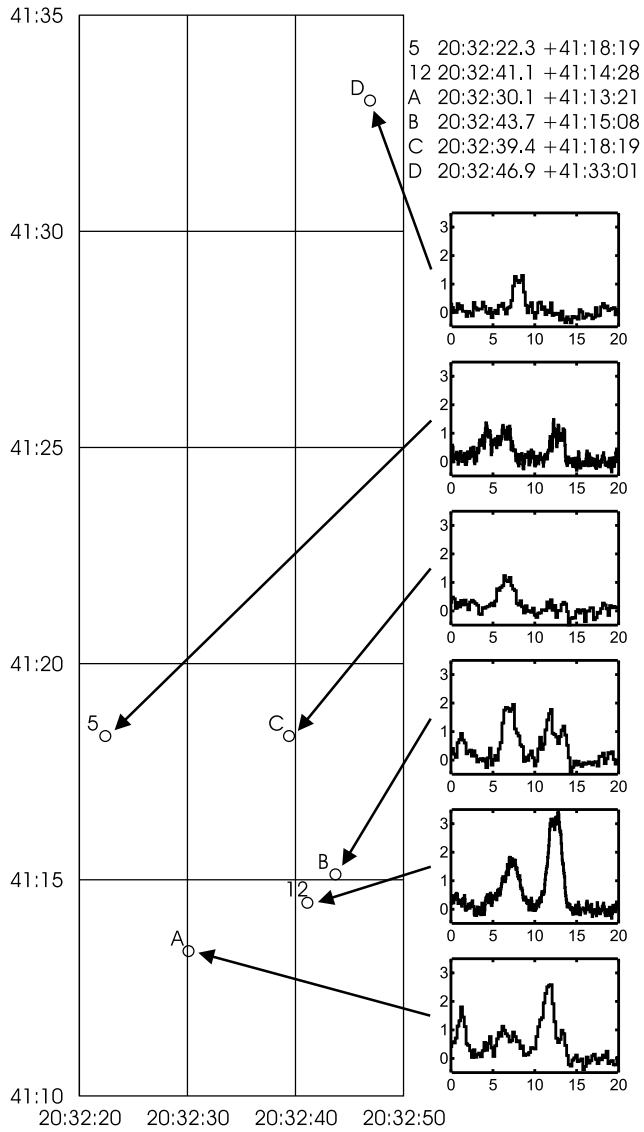

FIG. 6.—CO $J = 1$–0 "map" of the Cygnus OB2 association obtained at NRO. Spectra have T_A^* (K) as vertical axis, v_{LSR} (km s^{-1}) as horizontal axis. All coordinates are J2000.0.

and provide an upper limit of ~ 0.2 K for the $J = 1$–0 emission at the observed H_3^+ velocities. The closest reasonable velocity component is at $+25$ km s^{-1} and is only about 0.5 K. In contrast, Cygnus OB2 12 shows 3 K of emission.

During our 2001 May UKIRT run, we obtained an absorption spectrum of the R-branch of the CO $v = 1$–0 fundamental band. This spectrum (see Fig. 9 and Table 4) shows weak absorptions near $v_{LSR} \sim 25$ km s^{-1}, in agreement with the radio spectra. Because of the fairly small (geocentric) Doppler shift (~ 11 km s^{-1}) at the time of the observation, it is difficult to accurately measure the column density, but it is clear that the total CO column density is less than 10^{16} cm^{-2}. A previously obtained Phoenix spectrum of the $v = 2$–0 overtone band (from 1997 June) provides a less stringent upper limit on the total CO column density of $\sim 10^{17}$ cm^{-2}.

Both the radio and infrared results demonstrate that there is very little (if any) CO associated with the H_3^+ toward HD 183143.

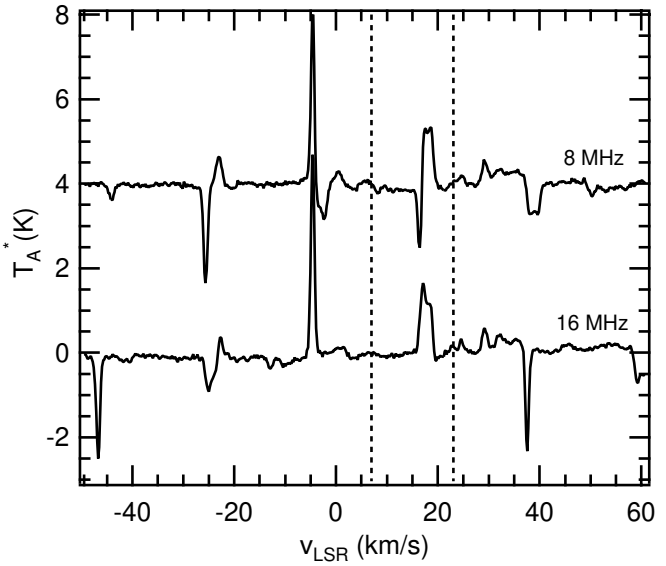

FIG. 7.—^{12}CO $J = 2$–1 frequency-switched spectra toward HD 183143, obtained at JCMT. The velocities of the H_3^+ lines are marked with vertical dashed lines.

3.4. CO *toward WR 104 and WR 118*

At UKIRT in 2001 May, we obtained spectra of the CO fundamental band toward the Wolf-Rayet stars WR 104 and WR 118. The spectra are shown in Figure 9, and the line parameters are listed in Table 4. WR 104 shows a single velocity component centered at $v_{LSR} \sim 21$ km s^{-1}—surprisingly, this is different from the velocity of the H_3^+ (~ 10 km s^{-1})! WR 118 has a very complicated velocity structure, which we have fitted with four Gaussian components. The lowest velocity component at $v_{LSR} \sim 10$ km s^{-1} may be associated with the H_3^+ component at $v_{LSR} \sim 5$ km s^{-1}, and the blended components near $v_{LSR} \sim 40$–55 km

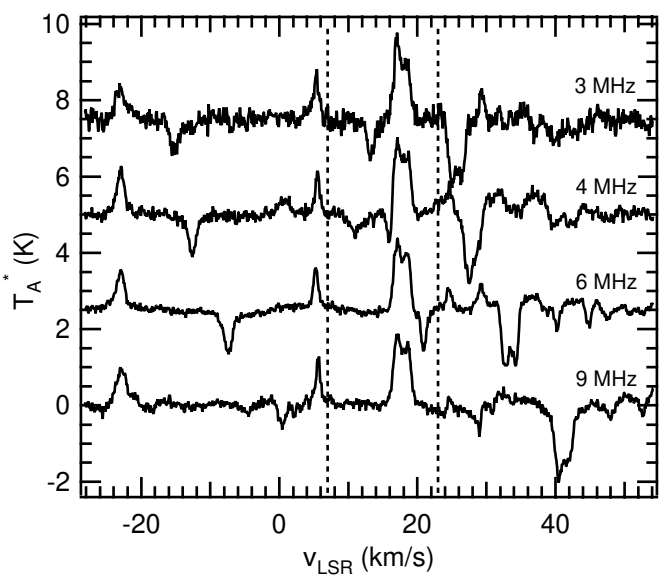

FIG. 8.—^{12}CO $J = 1$–0 frequency-switched spectra toward HD 183143, obtained at Nobeyama (folding has not been performed). The velocities of the H_3^+ lines are marked with vertical dashed lines.

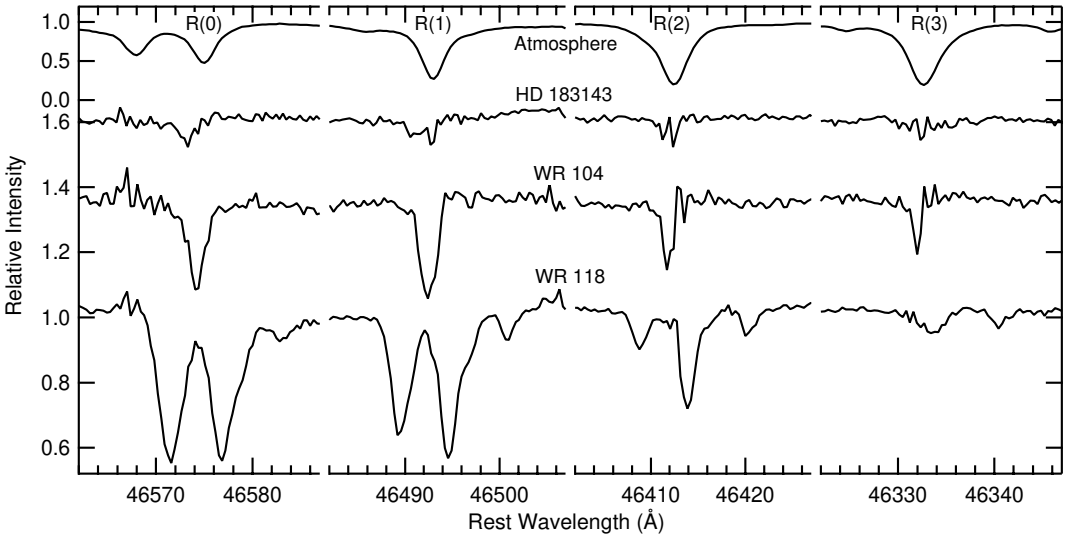

FIG. 9.—^{12}CO $v = 1$–0 fundamental band observations of HD 183143, WR 104, and WR 118, obtained at UKIRT. Object spectra have been ratioed by standard star spectra to remove the atmospheric CO lines.

s^{-1} are consistent with the second H_3^+ component at $v_{LSR} \sim 48$ km s^{-1}.

Without any radio spectra of these sources, it is difficult to attempt saturation corrections, so we have simply listed in Table 4 the column densities in the limit that the lines are optically thin. In this limit, WR 104 has $N(CO) \sim 9 \times 10^{15}$ cm^{-2} and WR 118 has $N(CO) \sim 4 \times 10^{16}$ cm^{-2} (in the $J = 0$–3 levels).

3.5. C_2 *Spectra*

The C_2 A-X $v = 2$–0 band was clearly detected toward Cygnus OB2 12 at McDonald, as shown in Figure 10. Each line appears as a clear doublet with a separation comparable to that of the CO, except for the $Q(8)$ line which is blended with $P(4)$. The equivalent widths were measured separately for the two velocity components, except for the $Q(8) + P(4)$ blend, for which only the total equivalent width could be measured. The contribution of $P(4)$ was estimated from the strength of $Q(4)$, which permitted an estimate of the $Q(8)$ equivalent width for the sum of the two velocity components. The $Q(10)$ line was contaminated by an atmospheric H_2O absorption line, and the spectra were ratioed by that of α Cep in order to remove the contribution of the telluric line. The derived C_2 line parameters (for each component separately, as well as for the total profile) for Cygnus OB2 12 are listed in Table 6. Column densities have been

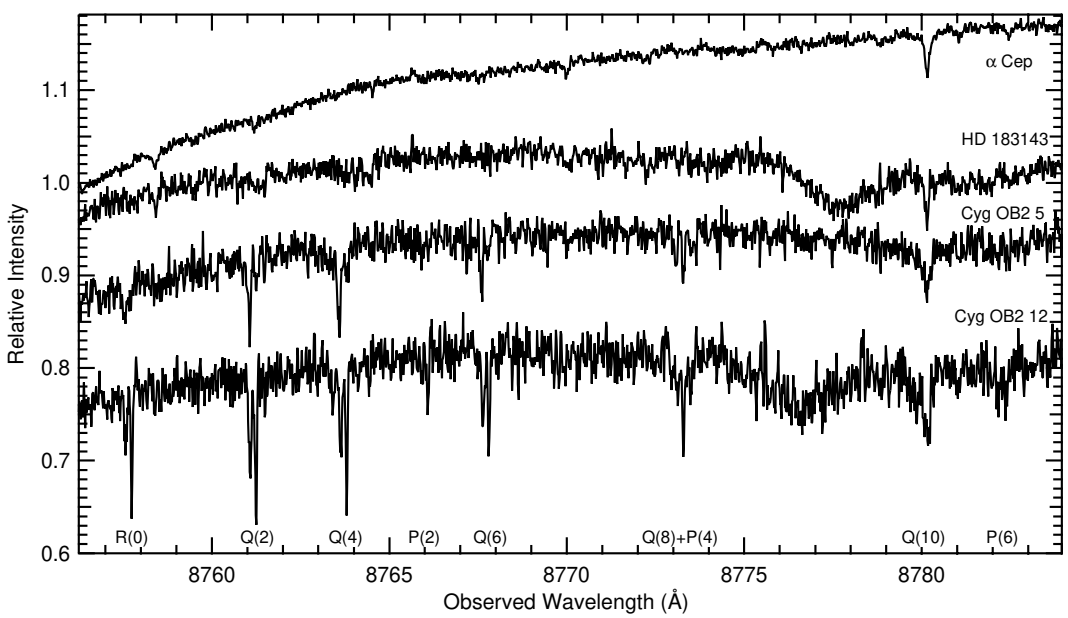

FIG. 10.—Spectra of the A-X $v = 2$–0 band of C_2 obtained at McDonald

TABLE 6

C_2 Line Parameters (Components Labeled as 1 and 2) for Cygnus OB2 12

Line	$W_\lambda^{1\,a}$ (mÅ)	$N(J)^1$ (10^{12} cm^{-2})	v_{LSR}^1 (km s^{-1})	FWHM^1 (km s^{-1})	$W_\lambda^{2\,a}$ (mÅ)	$N(J)^2$ (10^{12} cm^{-2})	v_{LSR}^2 (km s^{-1})	FWHM^2 (km s^{-1})	$W_\lambda^{tot\,a}$ (mÅ)	$N(J)^{tot}$ (10^{12} cm^{-2})
$R(0)$.....	4.96 ± 0.60	4.38 ± 0.53	6.7	2.8	6.87 ± 0.46	6.06 ± 0.41	12.6	1.7	11.83 ± 0.76	10.4 ± 0.7
$Q(2)$.....	9.91 ± 0.83	17.5 ± 1.5	6.7	3.1	10.67 ± 0.70	18.8 ± 1.2	12.4	2.2	20.58 ± 1.09	36.3 ± 1.9
$Q(4)$.....	8.97 ± 0.75	15.8 ± 1.3	6.6	3.2	9.65 ± 0.59	17.0 ± 1.0	12.3	2.0	18.62 ± 0.95	32.8 ± 1.7
$P(2)$.....	2.05 ± 0.60	...	6.8	2.0	3.38 ± 0.55	...	12.6	1.7	5.43 ± 0.81	...
$Q(6)$.....	7.40 ± 0.66	13.0 ± 1.2	6.6	3.1	7.33 ± 0.53	12.9 ± 0.9	12.2	2.0	14.73 ± 0.85	25.9 ± 1.5
$Q(8) + P(4)$...	...	...	...	...	...	...	...	...	19 ± 2^b	...
$P(4)^c$	...	...	...	...	...	...	...	...	6 ± 0.3	...
$Q(8)^d$	...	...	...	...	...	...	...	...	13 ± 2^b	22.3 ± 5.2
$Q(10)$	3.9 ± 0.6	6.6 ± 1.2	(6.7)^e	(3)^e	3.0 ± 0.5	5.3 ± 1.5	(12.5)^e	(2.1)^e	6.9 ± 0.8	11.9 ± 2.0

[a] Statistical uncertainties (1 σ) are listed unless otherwise noted. Systematic errors are difficult to estimate and may be larger.
[b] Estimate of systematic uncertainty.
[c] Estimated from $Q(4)$.
[d] Blend equivalent width minus $P(4)$ estimate.
[e] Values constrained in the fit to the ratioed spectrum.

determined assuming that the lines are optically thin, using the oscillator strength $f_{20} = 1.67 \times 10^{-3}$ of van Dishoeck (1983).

Using the method of van Dishoeck & Black (1982) and assuming the scaling factor for the radiation field $I = 1$ and the C_2-H_2 collisional cross section $\sigma_0 = 2 \times 10^{-16}$ cm^2, we can estimate the number density n of collision partners, as well as the kinetic temperature T. This analysis is performed by calculating the rotational distribution for a grid of points on the (n, T)-plane, then finding the best fit to the column densities $N(J)$ derived from the observed spectrum. The advantage of this method is that it yields the range of values of (n, T) that are consistent with the observations, given the uncertainties in the measurements.[11]

For the 7 km s^{-1} component, we obtain a best-fit value of (n, T) = (220 cm^{-3}, 40 K), and for the 12 km s^{-1} component we obtain (210 cm^{-3}, 30 K). Using the total column densities rather than those of the individual components yields (200 cm^{-3}, 30 K). These values are fairly well constrained by the observational data—it is exceedingly unlikely (i.e., it requires more than a 3 σ error in at least one of the measurements) that the density is outside the range 150–600 cm^{-3} or that the temperature is outside the range 25–55 K.

The spectrum of Cygnus OB2 5 also shows a hint of the doublet structure, but the signal-to-noise ratio of the spectrum is not sufficient to reliably measure the equivalent widths of the individual components. Therefore, we have measured only the total equivalent widths, which are reported in Table 7. An analysis of the rotational excitation (while very uncertain) suggests that the density exceeds 800 cm^{-3} and that the temperature lies in the range 60–90 K. According to Gredel & Münch (1994), chemical models predict a sudden decrease in C_2 abundance at densities above $10^{3.5}$ cm^{-3}. Taken with our (uncertain) results, this suggests that the density in the region where C_2 is found is in the range 800–3000 cm^{-3}.

In agreement with the results of Gredel (1999), we saw absolutely no trace of C_2 toward HD 183143. Assuming the $Q(2)$ line would have a width of ~ 5 km s^{-1}, the 3 σ limit on the equivalent width is about 1.7 mÅ, which corresponds to a column density of $N(J = 2) \lesssim 3 \times 10^{12}$ cm^{-2} (comparable to Gredel's upper limit), which is more than 10 times less than that of Cygnus OB2 12!

[11] A Web-based "C_2 calculator" is available at http://dib.uchicago.edu.

3.6. *Other Visible Spectra*

The results of our high-resolution visible spectroscopy are shown in Figure 11 (HD 183143), Figure 12 (Cygnus OB2 5), and Figure 13 (Cygnus OB2 12). These figures are plotted in velocity (with respect to the local standard of rest) and also display the infrared measurements of H_3^+ and CO.

CH appears as a doublet in Cygnus OB2 5, with velocities consistent with the infrared CO measurements. CH also appears as a doublet in HD 183143, with remarkably similar velocity structure to the H_3^+. The blue wavelength (4300 Å) of the CH transition made it inaccessible in the case of Cygnus OB 12 (which is very heavily reddened), but it may be possible to detect the line with a larger telescope such as the Hobby-Eberly Telescope. The line parameters of CH (as well as CH^+ and CN) are listed in Table 8. The CH

TABLE 7

C_2 Line Parameters for Cygnus OB2 5

Line	W_λ^a (mÅ)	$N(J)$ (10^{12} cm^{-2})
$R(0)$.....	6.6 ± 0.8	5.8 ± 0.7
$Q(2)$.....	10.7 ± 1.0	18.9 ± 1.8
$Q(4)$.....	13.5 ± 1.0	23.8 ± 1.8
$Q(6)$.....	8.0 ± 1.2	14.1 ± 2.1
$Q(8) + P(4)$.....	11 ± 3^b	...
$P(4)^c$	4.5 ± 0.3	...
$Q(8)^d$	7 ± 3^b	12.3 ± 5.3
$Q(10)^e$	1.5 ± 0.5	2.6 ± 0.9

[a] Statistical uncertainties (1 σ) are listed unless otherwise noted. Systematic errors are difficult to estimate and may be larger.
[b] Estimate of systematic uncertainty.
[c] Estimated from $Q(4)$.
[d] Blend equivalent width minus $P(4)$ estimate.
[e] Marginal feature; values very uncertain.

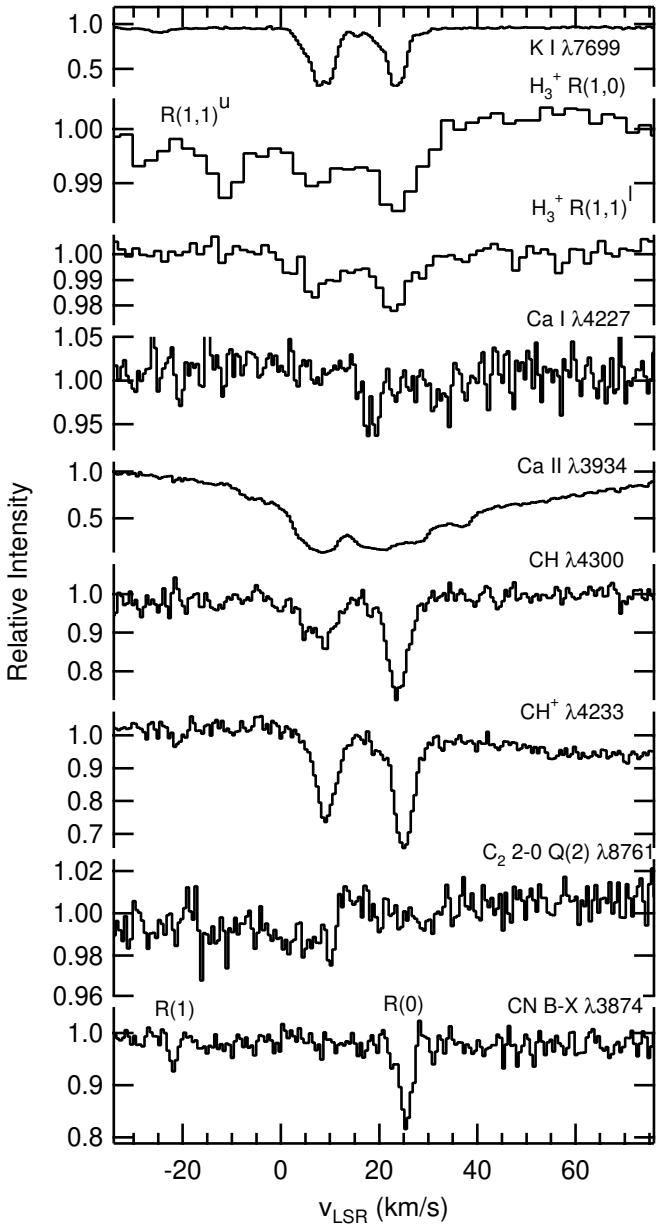

FIG. 11.—Summary of spectra of HD 183143, in velocity space

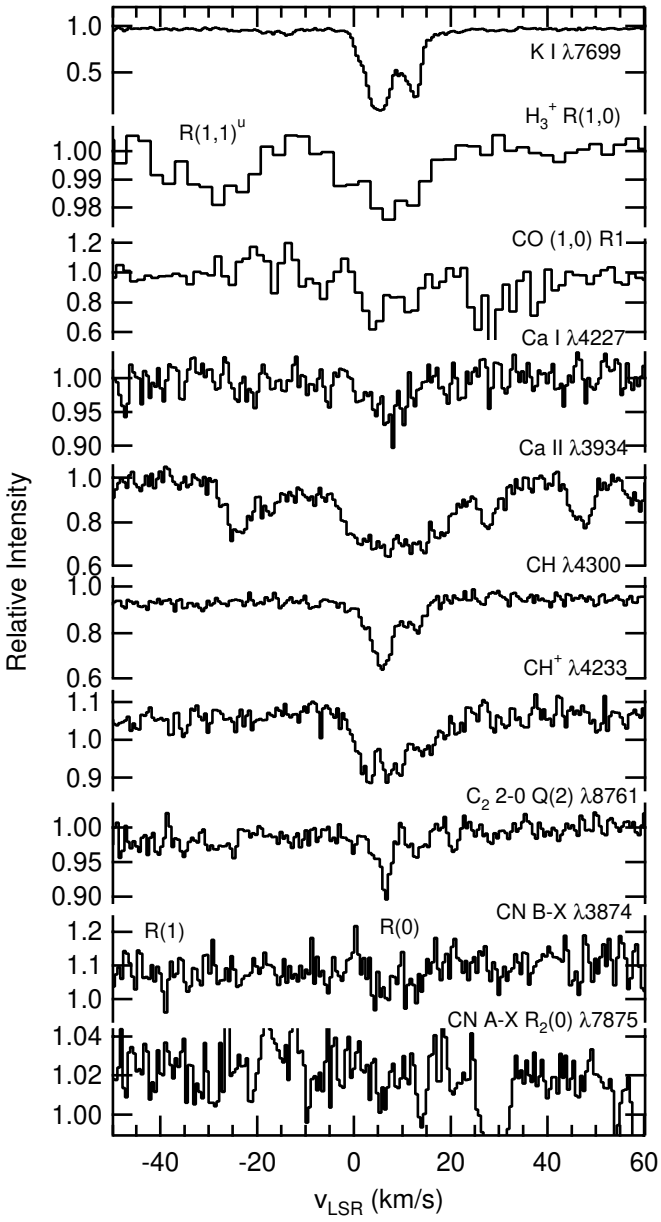

FIG. 12.—Summary of spectra of Cygnus OB2 5, in velocity space. The structure near 30 and 60 km s^{-1} in the lower trace is due to atmospheric lines.

column densities have been derived using the curve of growth of van Dishoeck & Black (1989), assuming $b = 1$ km s^{-1}.

It is interesting to compare the observed CH column densities with those that would be predicted from the empirical relation between H_2 and CH (Magnani & Onello 1995):

$$N(H_2) = 2.1 \times 10^7 N(CH) + 2.2 \times 10^{20} \text{ cm}^{-2} .$$

For HD 183143, $E(B-V) = 1.2$, so $N_H \sim 7 \times 10^{21}$ (assuming the standard gas-to-dust conversion factor; Bohlin, Savage, & Drake 1978), and (if $f \equiv 2N(H_2)/[N(H) + 2N(H_2)] = 2/3$) $N(H_2) \sim 2.3 \times 10^{21}$ cm^{-2}. From the empirical relation, one would then predict $N(CH) \sim 1.0 \times 10^{14}$, roughly twice the observed value. For Cygnus OB2 5, with $E(B-V) = 2.1$, we estimate $N(H_2) \sim 4 \times 10^{21}$ and therefore $N(CH) \sim 1.8 \times 10^{14}$ cm^{-2}, over 3 times the observed value. Assuming our choice of b-value is not too large, this suggests that these two sources may be somewhat different chemically from the usual diffuse cloud sources used to develop the empirical relation. However, this discrepancy may not indicate a drastic departure in chemical conditions, since other sources with lower color excess have been observed with similar departures from the empirical relations (Danks, Federman, & Lambert 1984). The CH discrepancy can be reduced by adopting a lower value of f, but this would decrease $n(H_3^+)$, exacerbating the problems discussed in § 4.2.

Another interesting molecule is CN: it is observed (marginally) as a doublet in both Cygnus OB2 12 (A-X) and in Cygnus OB2 5 (A-X and B-X). However, only one component (at $v_{LSR} \sim 25$ km s^{-1}) is observed toward HD 183143—whereas H_3^+, CH, and CH^+ all show two velocity

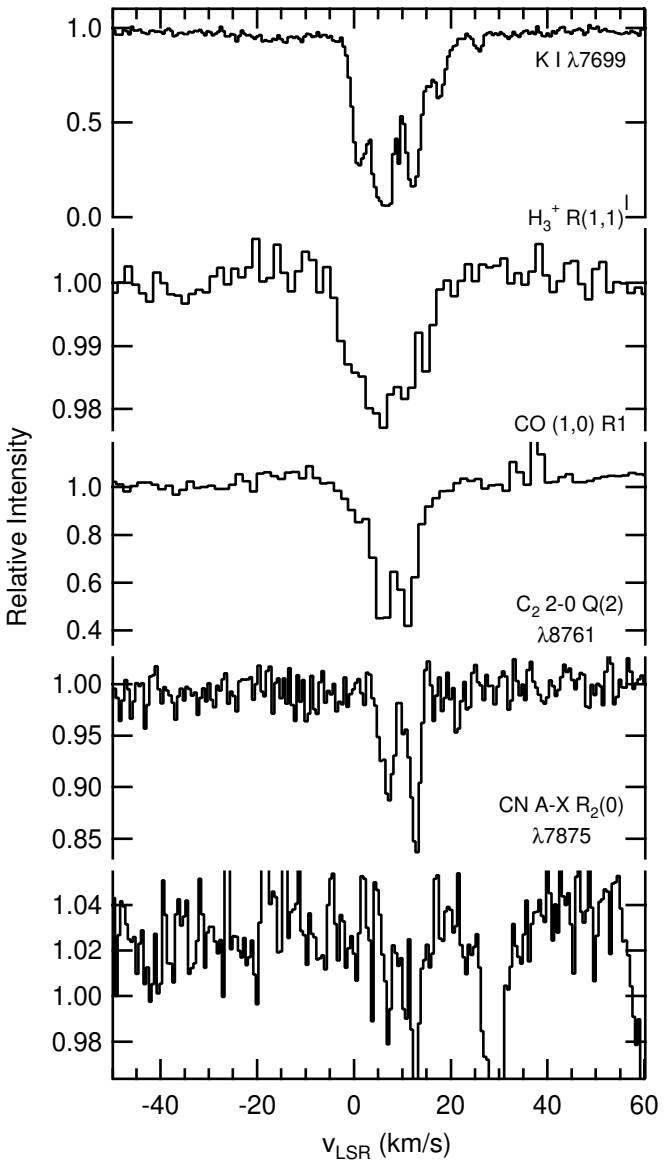

FIG. 13.—Summary of spectra of Cygnus OB2 12, in velocity space. The structure near 30 and 60 km s^{-1} in the lower trace is due to atmospheric lines.

components! The $R(1)$ line is also detected toward HD 183143, and the population of the $J = 0$ and $J = 1$ levels is consistent with the temperature of the cosmic microwave background.

Finally, it is worth noting that, at least in the case of Cygnus OB2 12 (Fig. 13), the velocity profile of H_3^+ appears more similar to that of K I than to C_2, CN, or CO. This could be because these three molecules are concentrated in the denser regions of the sight line, whereas H_3^+ (and K I) may exist over a larger path length.

4. DISCUSSION

4.1. *Model of* H_3^+ *Chemistry in Diffuse Clouds*

The formation of H_3^+, in dense or diffuse clouds, begins with the (cosmic-ray induced) ionization of H_2 to form H_2^+. The generally assumed rate of ionization is $\zeta \sim 3 \times 10^{-17}$ s^{-1}, so that the average H_2 gets ionized roughly once every 10^9 yr. Once ionized, the H_2^+ quickly reacts with another H_2 to form H_3^+ and an H atom. This ion-neutral reaction proceeds with the Langevin rate constant of 2×10^{-9} cm^3 s^{-1}, so that in a medium of H_2 density 100 cm^{-3}, the average H_2^+ must wait about 2 months to react to form H_3^+. Clearly, the initial ionization is the rate-limiting step, so we can say that H_3^+ is formed at a rate of $\zeta n(H_2)$.

The destruction of H_3^+ is very different in diffuse clouds, compared to dense clouds. In dense clouds, the dominant destruction path is an ion-neutral reaction with CO, with a rate constant of $\sim 2 \times 10^{-9}$ cm^3 s^{-1}. In diffuse clouds, electrons are very abundant (because of photoionization of C), so dissociative recombination dominates, with a rate constant of $k_e = 4.6 \times 10^{-6} T_e^{-0.65}$ cm^3 s^{-1} (Sundström et al. 1994).

Although the electrons produced by photoionization are probably formed at a high temperature (photons are available at energies up to 13.6 eV, and the ionization potential of C is only 11.3 eV), they will be quickly thermalized by collisions with H_2. Such collisions will occur with a Langevin rate constant (which scales as $\mu^{-1/2}$, where μ is the reduced mass) of $\sim 8 \times 10^{-8}$ cm^3 s^{-1}; in a medium with $n(H_2) = 100$ cm^{-3}, an electron experiences such a collision about once per day. The lifetime of the electron is limited by radiative recombination with C^+ ions, which occurs with a rate constant of $\sim 2 \times 10^{-11}$ cm^3 s^{-1} (Aldrovandi & Pequignot 1973) at the low temperatures (~ 30 K) of diffuse clouds. If $n(C^+) = 10^{-2}$ cm^{-3}, the average electron lifetime is about 10^5 yr. Evidently, the electrons will be very quickly thermalized to the kinetic temperatures of the clouds. The H_3^+ electron recombination rate constant is then $k_e \sim 5 \times 10^{-7}$ cm^3 s^{-1}, and the destruction rate of H_3^+ can be given as $k_e n(H_3^+) n(e)$.

To calculate the number density of H_3^+ (McCall et al. 1998a; Geballe et al. 1999), we make the steady-state approximation that the rates of formation and destruction are equal. Thus,

$$\zeta n(H_2) = k_e n(H_3^+) n(e) ,$$

which can be rearranged to give

$$n(H_3^+) = \frac{\zeta}{k_e} \frac{n(H_2)}{n(e)} .$$

The chemistry of H_3^+ is unique in the sense that the number density of H_3^+ is not dependent upon the number density of the cloud, but only on the ratio of the number densities of molecular hydrogen and electrons (as well as the ratio of two constants ζ/k_e). We can further simplify the above equation by considering f, the fraction of protons in H_2, writing $n(H_2) = (f/2)[2n(H_2) + n(H)] = (f/2)n(\Sigma H)$. Since most electrons are formed from the ionization of carbon, we can also write $n(e) = (1 - \alpha)n(\Sigma C)$, where α is the fraction of carbon in un-ionized (neutral or molecular) form. Finally, the gas-phase ratio of carbon atoms to hydrogen atoms is usually defined as $z_C \equiv n(\Sigma C)/n(\Sigma H)$. Putting this all together, we find

$$n(H_3^+) = \frac{\zeta}{k_e} \frac{f}{2} \frac{1}{1 - \alpha} \frac{1}{z_C} . \quad (1)$$

Adopting the values $\zeta = 3 \times 10^{-17}$ s^{-1}, $k_e = 5 \times 10^{-7}$ cm^3 s^{-1}, $f = 2/3$, $\alpha \sim 0$, and $z_C = 1.4 \times 10^{-4}$ (Cardelli et al. 1996; Sofia et al. 1997), we obtain

$$n(H_3^+) = 1.4 \times 10^{-7} \text{ cm}^{-3} . \quad (2)$$

TABLE 8

LINE PARAMETERS FOR CH, CH^+[a], AND CN[b]

Object	Species	Line	v_{LSR} (km s^{-1})	FWHM (km s^{-1})	W_λ[c] (mÅ)	N[c] (10^{12} cm^{-2})
Cyg OB2 5	CH	4300	5.6	6.0	26.5 ± 0.7	44.0 ± 1.2[d]
			12.7	3.4	7.1 ± 0.5	9.2 ± 0.6[d]
HD 183143.....	CH	4300	7.7	7.7	12.3 ± 0.7	17.0 ± 1.0[d]
			23.6	4.9	18.6 ± 0.6	27.7 ± 0.9[d]
Cyg OB2 5	CH^+	4233	2.6	5.0	11.2 ± 0.6	12.8 ± 0.7
			7.6	4.1	7.1 ± 0.6	8.1 ± 0.7
			13.3	8.9	11.8 ± 0.8	13.5 ± 0.9
HD 183143.....	CH^+	4233	9.0	4.9	18.3 ± 0.5	21.0 ± 0.6
			24.8	4.5	22.1 ± 0.5	25.3 ± 0.6
Cyg OB2 12.....	CN	A-X $R_2(0)$	6.8	1.1	1.3 ± 0.4	3.1 ± 1.0
			12.4	1.7	4.3 ± 0.6	10.3 ± 1.4
Cyg OB2 5	CN	A-X $R_2(0)$	5.6	2.0	1.2 ± 0.3	2.9 ± 0.7
			13.7	1.7	1.4 ± 0.3	3.4 ± 0.7
		B-X $R(0)$	5.6	3.9	4.1[e]	0.9[e]
			12.1	3.9	2.8[e]	0.6[e]
HD 183143.....	CN	B-X $R(0)$	25.2	2.5	5.6 ± 0.4	1.3 ± 0.1
		B-X $R(1)$	24.1	1.5	1.2 ± 0.2	0.4 ± 0.1

[a] For CH^+, we adopt the oscillator strength $f_{00} = 5.45 \times 10^{-3}$ of Larsson & Siegbahn 1983.
[b] For CN, we adopt the oscillator strengths $f_{00}^{BX} = 3.38 \times 10^{-2}$ (Larsson, Siegbahn, & Ågren 1983) and $f_{20}^{AX} = 7.6 \times 10^{-4}$ (Davis et al. 1986).
[c] Statistical uncertainties (1 σ) are listed unless otherwise noted. Systematic errors are difficult to estimate and may be larger.
[d] Estimated using the CH curve of growth of van Dishoeck & Black 1989, assuming $b = 1$ km s^{-1}. All other column densities computed assuming the lines are optically thin.
[e] These values are extremely uncertain because of the low flux of Cygnus OB2 5 at violet wavelengths.

The validity of the steady-state approximation can be checked by comparing the timescale needed to reach steady state with other relevant timescales. The timescale needed to achieve steady state is approximately the steady-state number density of H_3^+ divided by the formation rate, or $n(H_3^+)/[\zeta n(H_2)]$, which for $n(H_2) = 100$ cm^{-3} is about 1 yr—clearly much shorter than other relevant timescales!

4.2. *Inferred Cloud Parameters*

One cloud parameter can be determined from the H_3^+ observations independent of the chemical model—the kinetic temperature of the gas. This is possible because the ortho ($J = 1$, $K = 0$) and para ($J = 1$, $K = 1$) levels of H_3^+ are efficiently thermalized together through proton hop and proton exchange reactions with H_2 (McCall et al. 1998b). These reactions occur with the Langevin rate constant of 1×10^{-9} cm^3 s^{-1}, so that the average H_3^+ experiences such a reaction about every 4 months [assuming $n(H_2) = 100$ cm^{-3}]. The lifetime of the average H_3^+ can be estimated from the dissociative recombination rate k_e and the number density of electrons $n(e) \sim 10^{-2}$ cm^{-3} to be about 4.5 yr, considerably longer than the thermalization timescale. Therefore, we can use the Boltzmann expression

$$\frac{N_{\rm ortho}}{N_{\rm para}} = \frac{g_{\rm ortho}}{g_{\rm para}} e^{-\Delta E/kT} = 2e^{-32.87/T}$$

to estimate the kinetic temperature from the observed ortho:para ratio (in this equation, the g-values are the statistical weights). For Cygnus OB2 12, we obtain $T = 27 \pm 4$ K (McCall et al. 1998a); for Cygnus OB2 5, 47 ± 13 K; for HD 183143, 31 ± 3 K; for WR 104, 38 ± 10 K; and for the $+48$ km s^{-1} component of WR 118, 40 ± 3 K. (We cannot estimate the ortho:para ratio for the low-velocity component toward WR 118 because of the overlapping of the lines.)

Given our calculated number density of H_3^+ from the chemical model, we can now estimate the path length of absorption, using the relation $L = N(H_3^+)/n(H_3^+)$. Once the path length has been calculated, we can then estimate the average number density of collision partners along the path length as $\langle n \rangle = [N(H_2) + N(H)]/L$, where $N(H_2)$ and $N(H)$ can be estimated from the color excess and an assumed value of f (2/3). The results of this analysis are given in Table 9.

In most cases, the derived path lengths are a substantial fraction of the estimated distance to the star, which seems difficult to accept. In addition, the derived average number densities (for the sources in which H_3^+ was detected) are in the range 1–5 cm^{-3}, which seems unreasonably low. These densities are nearly 2 orders of magnitude lower than the densities typically derived from the rotational excitation of C_2. In addition, these densities are so low that a substantial fraction of H_2 should be photodissociated, meaning that our value of $f = 2/3$ should be lowered, which would in turn make the H_3^+ number density even smaller, the path lengths even longer, and the average density even lower.

It seems clear that there is a serious problem with the model and that $n(H_3^+)$ must be larger (probably by at least 1 order of magnitude) than we have calculated. In the next subsection, we explore possible solutions to this problem.

4.3. *Possible Solutions*

The equation for the number density of H_3^+,

$$n(H_3^+) = \frac{\zeta}{k_e} \frac{f}{2} \frac{1}{1-\alpha} \frac{1}{z_C}, \quad (3)$$

contains five parameters: the H_2 ionization rate (ζ), the dissociative recombination rate (k_e), the fraction of protons in molecular form (f), the fraction of carbon atoms that are not ionized (α), and the gas phase carbon fraction (z_C). We now consider each one of these parameters in more detail.

TABLE 9

CLOUD PARAMETERS BASED ON CONVENTIONAL CHEMICAL MODEL

Object	$N(H_3^+)$ (10^{14} cm^{-2})	L (pc)	d (pc)	$E(B-V)$ (mag)	$N(H_2)+N(H)$ (10^{21} cm^{-2})	$\langle n \rangle$ (cm^{-3})
Cyg OB2 12.....	3.8[a]	905	1700[b]	3.35[c]	12.95	4.8
Cyg OB2 5	2.6[d]	629	1700[b]	1.99[c]	7.69	4.1
HD 183143.....	2.3[d]	552	1000[e]	1.28[f]	4.95	3.0
HD 20041	3.5[g]	833	1400[e]	0.70[h]	2.71	1.1
WR 121	2.2[g]	524	1690[i]	1.68[j]	6.50	4.1
WR 104	2.3[d]	547	1300[i]	2.10[j]	8.12	4.9
WR 118	6.5[d]	1548	6300[i]	4.13[j]	15.97	3.4
HD 194279.....	<1.2[g]	<286	1100[e]	1.22[f]	4.72	>5.5
HD 168607.....	<0.6	<143	1100[e]	1.61[f]	6.23	>14.5
P Cygni	<0.6[g]	<143	1800[k]	0.63[k]	2.44	>5.7
χ^2 Ori.....	<0.7[g]	<171	1000[e]	0.44[l]	1.70	>3.3
ζ Oph.....	<0.4[g]	<86	140[m]	0.32[f]	1.24	>4.8

[a] From McCall et al. 1998a.
[b] Torres-Dodgen et al. 1991.
[c] From Schulte 1958.
[d] The UKIRT observations of $R(1, 0)$ and $R(1, 1)^u$ are adopted for these sources.
[e] Our estimate (spectroscopic parallax).
[f] From Snow et al. 1977.
[g] Total H_3^+ column density estimated to be twice that of para-H_3^+.
[h] Racine 1968.
[i] Smith et al. 1990.
[j] From Pendleton et al. 1994, assuming $R_V = A_V/E(B-V) = 3.1$.
[k] From Lamers et al. 1983.
[l] From the intrinsic color of Wegner 1994.
[m] From *Hipparcos* catalog (Perryman et al. 1997).

The fraction of protons in molecular form (f) has been assumed to have the value 2/3, which is the largest value found in the studies of molecular and atomic hydrogen by *Copernicus*, *IUE*, and *FUSE*. The maximum value of f is 1, so even making this adjustment (as is done in the model of Cecchi-Pestellini & Dalgarno 2000) will increase $n(H_3^+)$ only by a factor of 1.5—hardly enough to fix the problem. In addition, increasing the value of f would increase the discrepancy between inferred and measured N(CH), as discussed in § 3.6.

The gas phase carbon fraction (z_C) has been taken to be 1.4×10^{-4} based on ultraviolet observations of classical diffuse clouds (Cardelli et al. 1996; Sofia et al. 1997). Lowering this value (for instance, by assuming that a larger fraction of the carbon is depleted onto grains) would reduce the number density of electrons and therefore increase the number density of H_3^+. However, there is no astronomical evidence to support the magnitude of depletion necessary to mitigate the H_3^+ problem.

The fraction of carbon that is not ionized (α) has been assumed to be near zero. It is conceivable that a substantial fraction of the carbon could be in the form of neutral C atoms (rather than C^+), and there is no observational evidence (in these particular sight lines) that requires most of the carbon to be ionized. However, most chemical models of translucent clouds (see, for example, Fig. 9 of van Dishoeck & Black 1988) suggest that when the optical depth has increased to the point where $n(C) = n(C^+)$, over 10% of the carbon atoms are already in the form of CO. Taken along with our observations of a low column density of CO in these sight lines, this suggests that α must be less than 0.5 and thus could contribute at most a factor of 2 toward increasing the H_3^+ number density.

However, other models (e.g., Federman & Huntress 1989) suggest that the abundance of C^+ in an $A_V = 4$ cloud may be 15 times lower than in an $A_V = 1$ cloud. If we adopt this model, then it is possible that $\alpha \gtrsim 0.9$, which would increase $n(H_3^+)$ by 1 order of magnitude. Given the differences between the models, we hesitate to rely on them too much, in the absence of observational evidence. The best determination of the value of α would come from an observation of the C^+ transitions at 1334 and 2325 Å using the *Hubble Space Telescope* (*HST*).

Along the same lines, one might speculate about the possibility of an "electron sink" in these sight lines, so that C could still be ionized but the free electron abundance would be low. The best candidate mechanism for removing electrons from the gas is probably attachment to grains or large molecules (e.g., Lepp & Dalgarno 1988). However, because the number density of large molecules or grains is orders of magnitude lower than the number density of electrons (since these molecules or grains form from elements with cosmic abundance less than or equal to that of carbon, and each molecule or grain contains many atoms), this process could not effect the removal of a significant fraction of the electrons from the gas phase.

The H_2 ionization rate (ζ) has been assumed to be 3×10^{-17} s^{-1}, but this value is not terribly well constrained. Cecchi-Pestellini & Dalgarno (2000) assume 6×10^{-17} in order to increase the H_3^+ number density, and values as high as $\sim 2 \times 10^{-16}$ have been derived from analysis of the chemistry leading to OH in diffuse clouds (van Dishoeck & Black 1986). While the flux of high-energy ($\gtrsim$100 MeV) cosmic rays can be constrained by observations in the interplanetary medium, the flux of lower energy cosmic rays is essentially unconstrained, because of the influence of the Sun. If the cosmic-ray spectrum is assumed not to roll off too rapidly below 100 MeV, it is conceivable that ζ might be as high as 10^{-15} s^{-1} (Hayakawa, Nishimura, & Takayanagi 1961). A large flux

of low-energy cosmic rays might increase the H_3^+ number density in diffuse clouds while not seriously affecting the situation in dense clouds, into which the low-energy cosmic rays could not penetrate.

Other sources of H_2 ionization have also been suggested. Black (2000) has suggested that X-rays from the luminous stars in the Cygnus OB2 association could increase the effective ζ and therefore $n(H_3^+)$. While this suggestion might solve the problem for the sight lines toward Cygnus OB2, our observations of high $N(H_3^+)$ toward several other sources imply that a more general solution is needed. Black (2000) has also suggested that ultraviolet photoionization of H_2 might contribute. However, photoionization of H_2 requires photons with energies above 15.4 eV, which will ionize H atoms. While Black suggests that such photons could escape the H II region near the Cygnus OB2 giants, it seems unlikely that they could penetrate the boundaries of diffuse clouds, where H atoms are abundant. Furthermore, our new detections of H_3^+ again suggest that the sight lines toward the Cygnus OB2 association are not unique.

The last parameter in the equation for the H_3^+ number density is the dissociative recombination rate (k_e). In this work, we have adopted the value of $k_e = 4.6 \times 10^{-6} T_e^{-0.65}$ cm^3 s^{-1} derived from storage ring experiments (Sundström et al. 1994). However, the value of this constant has been the matter of great controversy over the past two decades—other experimental techniques currently yield a value of k_e that is about 1 order of magnitude lower (for a review of the field, see Larsson 2000). It has been suggested that the discrepancy might be due to stray fields present in the storage ring experiments and that the recombination rate under interstellar conditions could be quite low. To make matters worse, attempts to theoretically calculate the recombination rate yield rates more than an order of magnitude smaller than the smallest values obtained in experiments (Orel, Schneider, & Suzor-Weiner 2000), but it should be noted that the theory of this recombination process is not yet mature. Given the present uncertainty in the true value of k_e, it is possible that the problem of diffuse cloud H_3^+ may be solved on this front.

4.4. *Observational Tests*

The resolution of the mystery of diffuse cloud H_3^+ will most likely come from further observational work. First, we must determine with certainty whether the unexpectedly high number density of H_3^+ is a "local" problem (i.e., due to special conditions in these particular sight lines or this class of sight lines), or if it is a "global" problem. The present observational situation is summarized in Figure 14, which plots the observed H_3^+ column density (or the upper limit, denoted by a bar to zero) versus the color excess $E(B-V)$. In addition to the present observations, the detection of H_3^+ toward the Galactic center source GC IRS 3 (Geballe et al. 1999) has been added (the H_3^+ column density plotted is that of the narrow component attributed to diffuse clouds by Geballe et al. 1999, and the adopted color excess is that attributed to diffuse clouds by Whittet et al. 1997). Keeping in mind that

$$N(H_3^+) \sim n(H_3^+)L \propto n(H_3^+)\,\frac{E(B-V)}{\langle n_H \rangle}\,, \qquad (4)$$

the plot is not inconsistent with a constant $n(H_3^+)$ and small variations (of a factor of a few) in the average density $\langle n_H \rangle$. Therefore, at this stage there is no strong evidence that the "local" parameters (f, α, and z_C) are any different in the detection sources than they are in the nondetections such as ζ Oph.

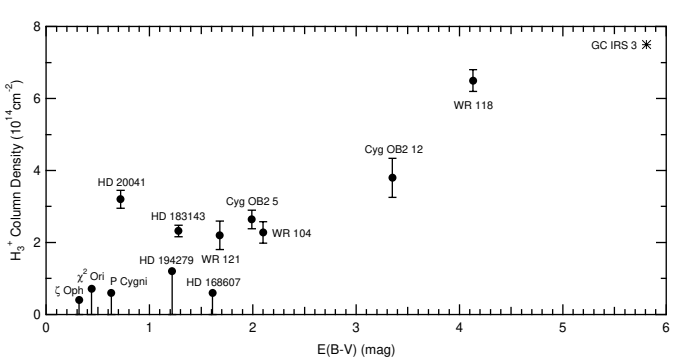

FIG. 14.—H_3^+ column density versus color excess

However, this inference needs to be tested directly by observations. This can be achieved by detecting H_3^+ along a line of sight with lower $E(B-V)$ that can be studied by *FUSE* and *HST*. Once the column densities of H_3^+, H I, H_2, C I, C II, CO, and CH are obtained for a single sight line, the influence of the "local" parameters will be directly determined.

Assuming that these parameters are found to have their canonical values, we will be left with the ratio ζ/k_e. Absent a speedy resolution from the experimenters or theorists in the field of dissociative recombination, further insight into these two constants can perhaps best be obtained through an observational survey of H_3^+ in more heavily reddened lines of sight. The rate of H_3^+ destruction is controlled by $n(e)/n_H$ (which depends on the optical depth in the ultraviolet), whereas the rate of H_3^+ formation is controlled by ζ (which, with a given incident cosmic-ray spectrum, depends on the stopping power of the cloud as a function of cosmic-ray energy). Therefore, a detailed study of the diffuse-to-dense cloud transition, along with chemical models, could help constrain the values of ζ and k_e. The highly reddened, early-type subset of the Stephenson catalog recently compiled by Rawlings, Adamson, & Whittet (2000) may serve as a good starting point for such a study.

5. CONCLUSIONS

The H_3^+ molecular ion has now been definitely detected in seven diffuse cloud lines of sight, suggesting that its unexpectedly high abundance is not due to the peculiarities of a particular region (the Cygnus OB2 association) but rather is a general feature of the diffuse interstellar medium. H_3^+ is observed in clouds with and without CO, C_2, and CN, confirming that the chemistry that leads to H_3^+ is completely decoupled from that which is responsible for these heavier diatomics. The most likely explanation for the high H_3^+ abundance is a larger than expected ζ/k_e ratio—due either to a larger flux of low-energy cosmic rays or to a lower value of k_e in interstellar conditions. The possibility of a lower than expected electron density has not been ruled out and should be directly tested by finding H_3^+ in a less reddened source.

The authors wish to acknowledge helpful discussions with D. G. York and L. M. Hobbs. We are grateful to the staffs of the various observatories that we have used, as well as to the respective telescope allocation committees. This

work has made use of the NASA Astrophysics Data Service, as well as the SIMBAD database at the Centre de Données astronomiques de Strasbourg. N. J. E. acknowledges support from the State of Texas and NSF grant 9988230. The University of Chicago portion of this work has been supported by NSF grant PHYS 97-22691 and NASA grant NAG5-4070. B. J. M. has been supported by the Fannie and John Hertz Foundation, and wishes to acknowledge a Sigma Xi Grant-in-Aid of Research and NOAO for travel support.

REFERENCES

Aldrovandi, S. M. V., & Pequignot, D. 1973, A&A, 25, 137
Black, J. H. 2000, Philos. Trans. R. Soc. London, A, 358, 2515
Bohlin, R. C., Savage, B. D., & Drake, J. F. 1978, ApJ, 224, 132
Cardelli, J. A., Meyer, D. M., Jura, M., & Savage, B. D. 1996, ApJ, 467, 334
Cecchi-Pestellini, C., & Dalgarno, A. 2000, MNRAS, 313, L6
Danks, A. C., Federman, S. R., & Lambert, D. L. 1984, A&A, 130, 62
Davis, S. P., Shortenhaus, D., Stark, G., Phillips, J. G., & Engleman, R., Jr. 1986, ApJ, 303, 892
Federman, S. R., & Huntress, W. T., Jr. 1989, ApJ, 338, 140
Geballe, T. R., McCall, B. J., Hinkle, K. H., & Oka, T. 1999, ApJ, 510, 251
Gredel, R. 1999, A&A, 351, 657
Gredel, R., & Münch, G. 1994, A&A, 285, 640
Hayakawa, S., Nishimura, S., & Takayanagi, T. 1961, PASJ, 13, 184
Herbst, E., & Klemperer, W. 1973, ApJ, 185, 505
Hobbs, L. M. 1973, ApJ, 181, 79
Huré, J. M., & Roueff, E. 1996, A&AS, 117, 561
Lambert, D. L., Sheffer, Y., & Crane, P. 1990, ApJ, 359, L19
Lamers, H. J. G. L. M., de Groot, M., & Cassatella, A. 1983, A&A, 128, 299
Larsson, M. 2000, Philos. Trans. R. Soc. London, A, 358, 2433
Larsson, M., & Siegbahn, P. E. M. 1983, Chem. Phys., 76, 175
Larsson, M., Siegbahn, P. E. M., & Ågren, H. 1983, ApJ, 272, 369
Lepp, S., & Dalgarno, A. 1988, ApJ, 335, 769
Magnani, L., & Onello, J. S. 1995, ApJ, 443, 169
McCall, B. J. 2000, Philos. Trans. R. Soc. London, A, 358, 2385
———. 2001, Ph.D. thesis, Univ. Chicago
McCall, B. J., Geballe, T. R., Hinkle, K. H., & Oka, T. 1998a, Science, 279, 1910
McCall, B. J., Geballe, T. R., Hinkle, K. H., & Oka, T. 1999, ApJ, 522, 338
McCall, B. J., Hinkle, K. H., Geballe, T. R., & Oka, T. 1998b, Faraday Discuss., 109, 267
McCall, B. J., & Oka, T. 2000, J. Chem. Phys., 113, 3104
Orel, A. E., Schneider, I. F., & Suzor-Weiner, A. 2000, Philos. Trans. R. Soc. London, A, 358, 2445
Pendleton, Y. J., Sandford, S. A., Allamandola, L. J., Tielens, A. G. G. M., & Sellgren, K. 1994, ApJ, 437, 683
Perryman, M. A. C., et al. 1997, A&A, 323, L49
Racine, R. 1968, AJ, 73, 233
Rawlings, M. G., Adamson, A. J., & Whittet, D. C. B. 2000, ApJS, 131, 531
Schulte, D. H. 1958, ApJ, 128, 41
Smith, L. F., Shara, M. M., & Moffat, A. F. J. 1990, ApJ, 358, 229
Snow, T. P., York, D. G., & Welty, D. E. 1977, AJ, 82, 113
Sofia, U. J., Cardelli, J. A., Guerin, K. P., & Meyer, D. M. 1997, ApJ, 482, L105
Sundström, G., et al. 1994, Science, 263, 785
Torres-Dodgen, A. V., Carroll, M., & Tapia, M. 1991, MNRAS, 249, 1
van der Hucht, K. A., et al. 1996, A&A, 315, L193
van Dishoeck, E. F. 1983, Chem. Phys., 77, 277
van Dishoeck, E. F., & Black, J. H. 1982, ApJ, 258, 533
———. 1986, ApJS, 62, 109
———. 1988, ApJ, 334, 771
———. 1989, ApJ, 340, 273
Watson, W. D. 1973, ApJ, 183, L17
Wegner, W. 1994, MNRAS, 270, 229
Whittet, D. C. B., et al. 1997, ApJ, 490, 729